Annals of Biomedical Engineering, Vol. 29, pp. 109–120, 2001
Printed in the USA.

0090-6964/2001/29(2)/109/12/$15.00

Factors Influencing Blood Flow Patterns in the Human Right Coronary Artery

J. G. MYERS,[1] J. A. MOORE,[1] M. OJHA,[2] K. W. JOHNSTON,[2] and C. R. ETHIER[1]

[1]Department of Mechanical and Industrial Engineering, and the [2]Institute of Biomaterials and Biomechanical Engineering, University of Toronto, Toronto, Ontario, Canada

(Received 15 February 2000; accepted 19 December 2000)

Abstract—Evidence suggests that atherogenesis is linked to local hemodynamic factors such as wall shear stress. We investigated the velocity and wall shear stress patterns within a human right coronary artery (RCA), an important site of atherosclerotic lesion development. Emphasis was placed on evaluating the effect of flow waveform and inlet flow velocity profile on the hemodynamics in the proximal, medial, and distal arterial regions. Using the finite-element method, velocity and wall shear stress patterns in a rigid, anatomically realistic model of a human RCA were computed. Steady flow simulations ($Re_D = 500$) were performed with three different inlet velocity profiles; pulsatile flow simulations utilized two different flow waveforms (both with Womersley parameter=1.82, mean $Re_D = 233$), as well as two of the three inlet profiles. Velocity profiles showed Dean-like secondary flow features that were remarkably sensitive to the local curvature of the RCA model. Particularly noteworthy was the ''rotation'' of these Dean-like profiles, which produced large local variations in wall shear stress along the sidewalls of the RCA model. Changes in the inlet velocity profiles did not produce significant changes in the arterial velocity and wall shear stress patterns. Pulsatile flow simulations exhibited remarkably similar cycle-average wall shear stress distributions regardless of waveform and inlet velocity profile. The oscillatory shear index was very small and was attributed to flow reversal in the waveform, rather than separation. Cumulatively, these results illustrate that geometric effects (particularly local three-dimensional curvature) dominate RCA hemodynamics, implying that studies attempting to link hemodynamics with atherogenesis should replicate the patient-specific RCA geometry.
[DOI: 10.1114/1.1349703]

Keywords—Hemodynamics, Right coronary artery, Atherogenesis, Numerical modeling, Wall shear stress

INTRODUCTION

Occlusion of large and medium size arteries due to atherosclerotic plaque formation and rupture is an important cause of morbidity and mortality.[28] Although many systemic risk factors for atherogenesis exist, plaques tend to develop at specific locations, an observation that has led to the ''geometric risk factor'' hypothesis for atherogenesis.[12] In particular, low and oscillating wall shear stresses (WSSs) have been associated with atherosclerotic lesions within the coronary arteries,[1,12,17] carotid arteries,[18] and the abdominal aorta.[40] The putative link between WSS and atheroma is consistent with other findings, including the ability of endothelial cells to transduce mechanical forces[6] and the role of WSS in the regulatory adaptation of arterial lumen caliber.[42] However, this association is not unambiguous, due in part to the tendency of other factors such as impaired mass transport[4] to co-localize with regions of low WSS. Thus, the link between atherogenesis and local hemodynamic factors requires further investigation.

The coronary arteries are a common and important site of atherosclerotic plaque formation. Despite the clinical importance of the coronaries, relatively little is known about hemodynamic features in these arteries due in part to the difficulty of studying blood flow in the coronary arteries. Most studies of coronary artery hemodynamics have concentrated on the left anterior descending (LAD) artery and its main bifurcation,[11,13,32] with fewer studies of the right coronary artery (RCA).[17,36] Several studies have shown that the human RCA preferentially exhibits atherogenesis in regions proximal to the acute margin,[1,17,29] where hemodynamic features (affected by a combination of geometric, pulsatility, and inlet velocity profile parameters) are expected to be complex.

Factors influencing RCA hemodynamics can be divided into five categories: vessel geometry, branch flows, vessel movement and compliance, flow waveform shape, and shape of the inlet (ostium) velocity profile. We briefly review what is known about the first three of these factors. The complex three-dimensional geometry of coronary arteries, including their compound curvature,[3] markedly influences flow, and WSS patterns.[7,17,32] Studies of the main bifurcation in the LAD have shown flow separation and recirculation regions

Address all correspondence to Professor C. Ross Ethier, Department of Mechanical and Industrial Engineering, 5 King's College Road, University of Toronto, Toronto, Ontario M5S 3G8, Canada; electronic mail: ethier@mie.utoronto.ca

that intensify WSS variations across the LAD.[10,19,32] Myocardial-induced coronary artery motion during the cardiac cycle can cause temporal variations in curvature of up to 80%,[30] which is expected to influence WSS patterns.[20,37,38] In addition, coronary artery compliance can substantially influence the WSS magnitude and oscillations across the arterial circumference.[35]

Less well understood are the roles that flow waveform and inlet (ostium) velocity profile have on coronary artery hemodynamics. Mark and co-workers[21] demonstrated the importance of unsteadiness in a LAD flow phantom but did not compare the effects of different flow waveforms. In other arteries (e.g., in the aortic arch[5]), flow waveform is known to have an important effect. The ostium velocity profile, determined by the interaction between aortic and coronary artery hemodynamics, does not appear to have been studied. However, it is known that in simple curved tube systems, inlet velocity profile markedly influences the initial development of the flow field.[39]

Our interest is in investigating the link between atherosclerotic plaque formation and hemodynamics in the coronary arteries. A key requirement of such an investigation is the ability to characterize velocity and WSS patterns accurately in the coronary arteries. In this study, we used computational fluid dynamic (CFD) techniques to study flow and WSS patterns in an anatomically faithful model of a human RCA. Our specific focus was on describing the effects of flow waveform and ostium velocity profile. The model was assumed to be static and branch flows were not considered. Primary velocity, secondary velocity, WSS, and oscillating WSS patterns along the length of the RCA were examined and compared with previously published results.[17]

MATERIALS AND METHODS

Model Construction

A digital representation of a human RCA was derived from computer tomographic (CT) scans of the anatomically realistic acrylic flow model analyzed experimentally by Kirpalani and co-workers.[17] In brief, the heart of a 47-year-old woman who died from non-vascular-related causes was obtained at autopsy. The RCA, while intact on the heart and still attached to the aorta, was flushed with saline. A catheter introduced into the ostium of the RCA was used to fill the RCA with Batson's No. 17 Corrosion Casting Compound (Polysciences, Warrington, PA) at a pressure of 100 mm Hg. The entire heart, with the RCA still attached, was then fixed in 10% buffered formalin for 2 days. After polymerization of the casting compound, the RCA was excised from the heart, photographed, demarcated for orientation (epicardial, myocardial, distal, and proximal), and sliced axially along the inner surface of the main curvature to allow cast removal. Morphometric examination of the artery showed that the wall exhibited minimal atherosclerotic lesions and intimal thickening. Comparison of the lumen cast and the RCA photographs indicated that approximately the first 2 cm of the RCA were not cast; that is, the cast ''origin'' was approximately where the RCA joined the myocardial surface.

Flow phantom construction continued by first creating an intermediate, flexible, negative mold of the RCA cast and then using this to create a sacrificial, positive cast constructed of a low melting point alloy (Cerrolow® -117, Cero Metal Products, Bellefonte, PA). Next, the daughter branches on the positive cast were removed, and the cast was polished. Methyl methacrylate (Polyscience, Inc.) was polymerized around the positive alloy cast, which was then heated to 60 °C to remove the low melting point alloy and create the flow phantom geometry. Final preparation of the phantom involved polishing to an optical finish, milling appropriately sized inlet and outlet flow sections, and attaching flow connectors.

A series of CT scans, roughly parallel to the ventral plane, were made along the flow phantom geometry using a high-resolution radiographic CT-imaging system.[14] Each image in the set had an isometric resolution of 230 μm. A computer-aided design (CAD) model of the RCA lumen was then constructed using a modification of previously published techniques.[24] In brief, the arterial boundaries of the CT image slices were segmented with an in-house application written for the MATLAB™ programing environment and utilizing the MATLAB™ Image Processing Toolbox (MathWorks, Natick, MA). By approximating the arterial path from the original series of CT images, an updated set of image slices, perpendicular to the local arterial axis, was constructed from the original imaging data. Segmenting the artery edge from these oblique slices generated a representation of the lumen surface structure. For this study, 250 axial slices and two-dimensional lumen contours were made with the original image set, resulting in an axial resolution of approximately 500 μm. This resolution was lower than that of the CT images, but provided a good balance between the accuracy of the CT images and the capabilities of the software used for solid model reconstruction. The segmented contours were smoothed,[25] imported to a commercial CAD package (DDN, Fluent Inc., Lebanon, NH), and used to construct a B-spline surface (Fig. 1). The inlet diameter (D) was 1.94 mm and the outlet diameter was 1.70 mm.

To accommodate finite-element method (FEM) flow modeling, straight inlet and outlet extensions with circular cross section were added to the RCA geometry. The augmented model had a 5-diameter (5D)-long inlet section, placed upstream of the RCA cast origin, of which 4.5D was constructed with lofted CT image contours obtained from the inlet section of the flow phantom. The

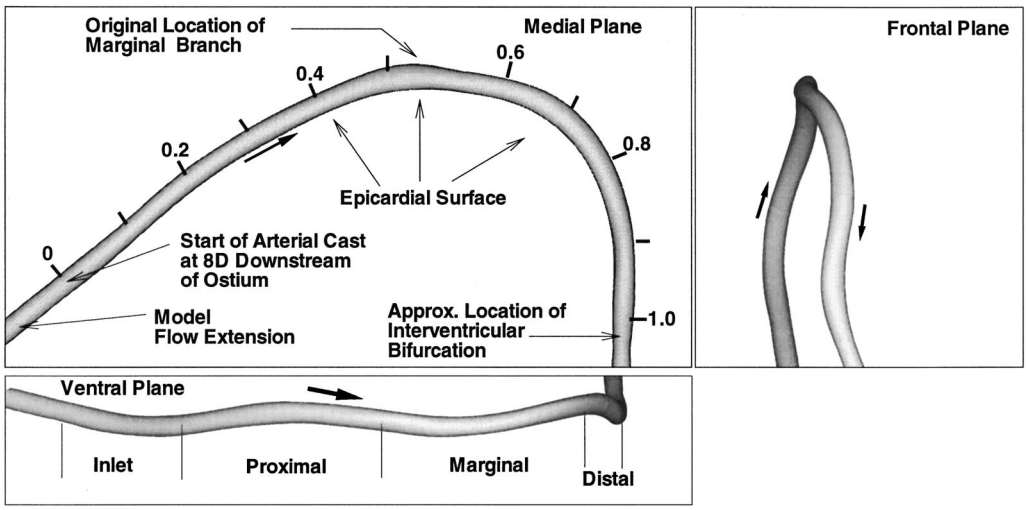

FIGURE 1. Medial, frontal, and ventral plane views of the RCA model. This physiologically accurate geometry exhibits variations in three-dimensional curvature and caliber along the arterial path. Four regions are specified to characterize the geometry (specified from 0 to 1.0 in the medial plane). The inlet region: 0%–20% of the cast length (0D–7.3D); proximal region: 20%–50% of the cast length (7.3D–18.3D); marginal region: 50%–75% of the cast length (18.3D–27.5D); and distal region: 75%–100% of the cast length (27.5D–36.6D).

remaining 0.5D section, including the inlet plane, was constructed by projecting a circular contour along the normal of the last profile position upstream of the cast origin. This, in effect, placed the model inlet 2 to 3D distal to the ostium's estimated position. A straight 15D outlet extension was constructed by first forming a 5D section downstream of the RCA cast limit with the CT image contours of the flow model's outlet section. The remaining 10D section was formed by projecting circular contours, placed at every 0.5D from the last outlet image position, along the average direction estimated from the last ten lofted profiles.

Numerical Flow Simulations

Finite-element meshing was carried out with the commercial code GEOMESH (Fluent Inc., Lebanon, NH). In this process, a body-fitted mesh was first generated based on user-defined nodal distributions specified for the RCA geometry. A volume mesh was then generated from this surface mesh via Delaunay triangulation. A well-validated, in-house three-dimensional (3-D), incompressible Navier–Stokes flow solver was used to perform the hemodynamic simulations in this study.[8,23] Newtonian blood rheology was assumed. No-slip boundary conditions were applied at the artery walls, and a zero-traction condition was imposed at the model outlet. Three inlet velocity conditions were utilized in this study:

(1) A fully developed inlet velocity profile. Both steady (Poiseuille velocity profile) and unsteady (Womersley velocity profile) flow simulations were performed with this inlet condition [Fig. 2(a)].
(2) A ''blunt'' inlet velocity profile, with constant axial velocity component for $0 \leqslant a/r \leqslant 0.8$, and a linear reduction in velocity to the wall in the region 0.8

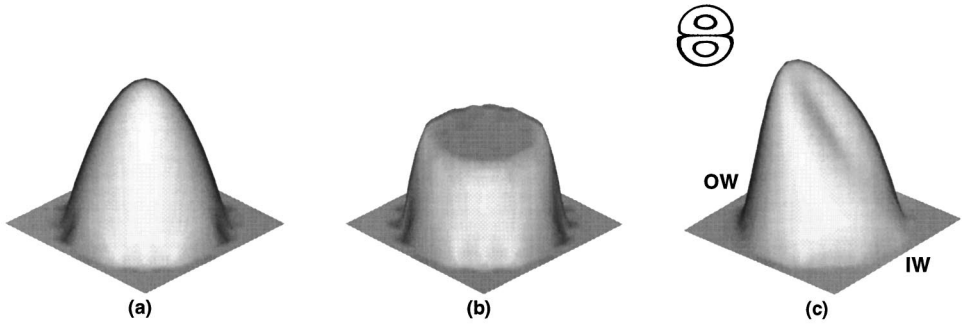

FIGURE 2. Inlet profiles used in steady flow simulations: (a) a fully developed (Poiseuille), (b) a blunt (or flat), and (c) a fully developed Dean-type flow. The Dean profile is characterized by an axial velocity distribution shifted toward the outer wall of curvature and a paired-vortex secondary flow structure, as illustrated above and to the left of (c).

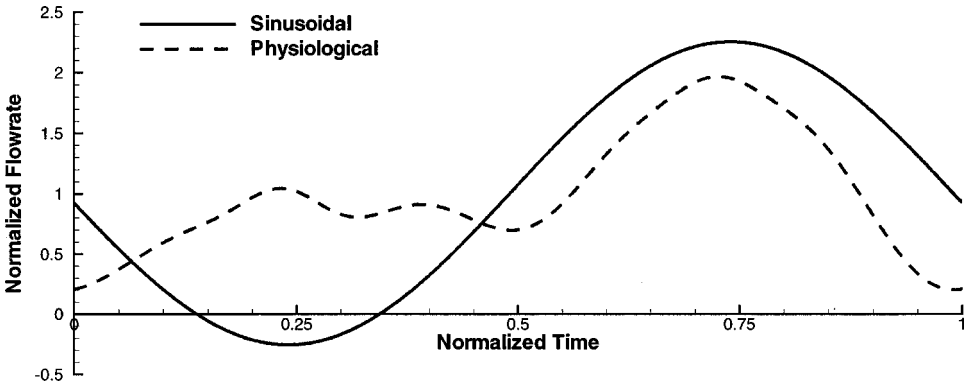

FIGURE 3. The two flow waveforms used in this study. The sinusoidal waveform follows the work of Kirpalani *et al.* (Ref. 17). The physiological waveform was based on the work of Matsuo *et al.* (Ref. 22), who measured the waveform in healthy patients using a Doppler flowmeter catheter. Both waveforms were normalized to the same mean (Re_D=233) and had the same Womersley unsteadiness parameter, α=1.82.

$\leqslant a/r \leqslant 1.0$, where a/r is the dimensionless radial position [Fig. 2(b)]. Both steady and unsteady flow simulations were performed with this inlet condition.

(3) A fully developed Dean-type velocity profile.[31] This profile exhibits a pair of symmetric counter-rotating Dean-type secondary vortices and an offset axial profile, shifted toward the outer wall of curvature as viewed from the medial plane [Fig. 2(c)]. The profile corresponded to the small Dean number limit[31] ($[a/R]^{1/2}*Re_D=36$, where R is the radius of curvature), which assumed a gently curving section preceding the straight extension section of the arterial model. Unsteady simulations were not performed with this inlet condition.

Each of these inlet conditions was used in a steady flow simulation for a Reynolds number (Re_D) of 500, based on inlet diameter and mean inlet velocity. This steady flow Re_D, which is somewhat higher than the mean resting Re_D in the RCA, corresponds to the peak Re_D in the flow cycle under resting conditions. It is also representative of the mean Re_D in the coronary arteries during periods of moderate exercise.[33] Pulsatile flow simulations utilized inlet velocity profiles (1) and (2), modulated in time by one of the following two unsteady flow waveforms (Fig. 3): (1) a sinusoidal waveform;[17] and (2) a physiologically relevant waveform obtained from healthy patient measurements with a Doppler flowmeter catheter.[22] Both unsteady flow waveforms had a time-mean $Re_D=233$ and $\alpha=1.82$.

During postprocessing of the unsteady flow simulations, an oscillatory shear index (OSI), generalized for three dimensions, was calculated to quantify cyclic variations of WSS. The formulation we have used corresponds to that developed by Moore *et al.*[26] and represents the interval of the flow cycle that the local shear vector points more than 90° from the mean shear direction, weighted by the local shear magnitude.

RESULTS

Geometric Characterization

Data are presented in terms of a normalized axial position along the artery, where the RCA cast origin is chosen as the reference station (0 position) and the RCA cast centroidal path length (69.5 mm, 36.6D) is chosen as the reference length (L). The four regions defined in Fig. 1 were used to characterize the RCA geometry: (1) the inlet region, (2) the proximal region, (3) the marginal region, and (4) the distal region.[17] Due to the significant curvature in the medial plane, curvature in this plane was termed the ''primary'' curvature of the model, while ''out of (medial) plane'' curvatures were called ''transverse'' or ''secondary'' curvatures. Our focus is on two specific regions related to the primary curvature of the RCA, the inner wall (epicardial surface) and outer wall (pericardial surface). Further characterization of the arterial geometry is discussed in a companion paper.[15]

Mesh Independence

Mesh independence was investigated by comparing steady flow WSS (fully developed inlet condition) in meshes with 57,850, 167,607, and 357,643 nodes (Fig. 4). The WSS distributions show some mesh dependence along the RCA outer wall, with the 167,607 and 357,643 noded models exhibiting similar trends and WSS magnitudes. Along the RCA inner wall, which is the most significant region from a clinical perspective, the WSS distributions differ only slightly between the two densest meshes and can be considered essentially fully resolved. A more detailed adaptive mesh study using only a single set of steady inlet conditions[34] indicated that the rms WSS error in the 167,607 node mesh was approximately 6% on the inner wall and 16% on the outer wall. The errors in WSS are expected to be slightly higher for unsteady flow simulations, since unsteady effects tend to

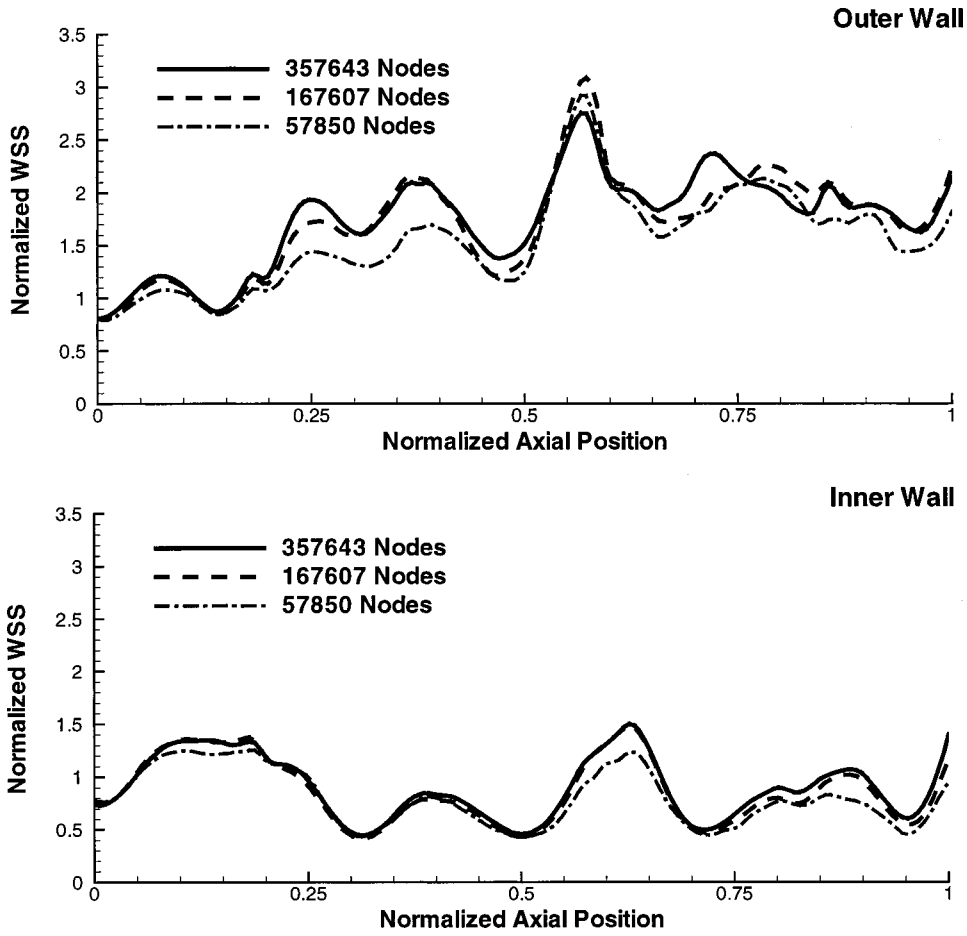

FIGURE 4. Mesh independence study in the RCA model. The steady WSS, normalized by the inlet Poiseuille value of 27 dyn cm^{-2}, is plotted vs normalized arterial length along the outer (upper panel) and inner (lower panel) RCA walls. The parabolic inlet velocity profile was used in each case.

localize in the near-wall region. Considering all factors, we felt that the 167,607 node mesh represented an acceptable balance between computational cost and model accuracy for the goals of this study, and therefore this mesh was used for all production runs. We accept that modest errors can be expected in the results along the outer wall, but feel that increased mesh resolution is unlikely to change the conclusions of this study.

Steady Flow Modeling: Variations due to Inlet Velocity Profile

All steady flow simulations exhibited similar flow patterns, such as a general displacement of the higher momentum fluid to the outer wall. Secondary, nonsymmetric Dean-type helical flow patterns, driven by the primary and secondary arterial curvature, strengthened as the flow developed, with velocities up to 15% of the maximum axial velocity (Fig. 5). An interesting observation was the ''rotation'' of these Dean-type velocity profiles, which correlated with (and were presumably due to) the presence of secondary curvature in the model (Fig. 5). This ''rotation'' in turn led to appreciable local variations in wall shear stress (Fig. 6), which contributed to the presence of local maxima and minima in the WSS pattern along the inner and outer walls (Fig. 6).

As illustrated in Fig. 5, the inlet velocity profile affected velocity patterns in the inlet and proximal regions of the RCA. However, the parabolic and blunt inlet velocity profiles quickly responded to the local arterial geometry, resulting in indistinguishable velocity profiles and secondary flow patterns by 0.25L. In contrast, the influence of the Dean-type inlet velocity profile on the velocity field persisted up to 0.4L, although the secondary flow patterns were similar to those for the other inlet conditions as early as 0.1L.

As expected, WSS values along the RCA's inner wall were generally lower than those found along the outer wall (Fig. 7). The most noteworthy effects of inlet velocity profile on WSS patterns occurred in the inlet and proximal regions:

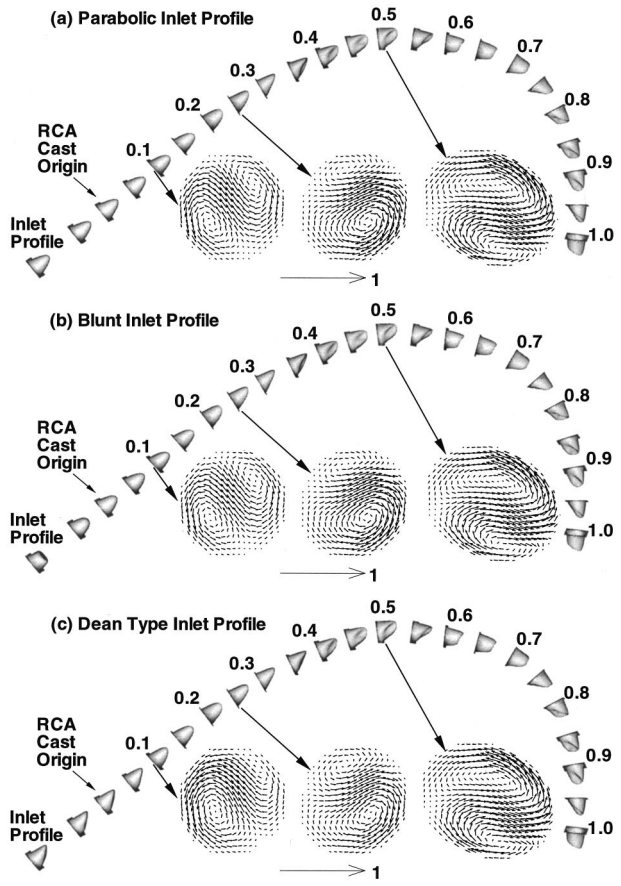

FIGURE 5. Steady flow velocity profiles at every 2D along the model length for the (a) parabolic, (b) blunt, and (c) Dean-type inlet profiles. Plotted surfaces are a visual representation of total fluid displacement according to the relationship $(x',y',z')=(x,y,z)+\text{const}^*(u,v,w)$, where (x,y,z) is a point on a plane cutting through the RCA model and (x',y',z') represents a point on the plotted surface. Secondary flow patterns at axial locations of 0.1, 0.25, and 0.5 of the arterial cast length are also shown. Note positions of individual profiles are specified in relation to the arterial cast origin.

(1) Inlet region: WSS distributions for the blunt and parabolic inlet profiles were very similar, differing by less than 10% of the inlet Poiseuille magnitude and exhibiting small, negative differences between outer and inner wall WSS magnitude. In contrast, WSS values from the Dean inlet velocity profile were as much as 60% higher (outer wall) and 25% lower (inner wall) than those from the parabolic inlet velocity profile (relative to the inlet Poiseuille magnitude), with somewhat larger ΔWSS, where $\Delta\text{WSS}=\text{WSS}_{\text{outerwall}}-\text{WSS}_{\text{innerwall}}$. However, these WSS differences were less pronounced beyond the inlet section (0.2L).

(2) Proximal region: WSS distributions for the parabolic and blunt inlet velocity profiles were indistinguishable in this region. The WSS distribution for the Dean-type profile still differed by as much as 20% (relative to inlet Poiseuille value) from the parabolic inlet distribution, although the inner wall showed much less deviation. Despite these differences in WSS magnitude, each simulation responded similarly to the increasing curvature with lower WSS on the inner wall and relatively large ΔWSS.

(3) Marginal and distal regions: All three inlet velocity profiles gave effectively identical WSS distributions in these regions. In general, along both the inner and outer walls, peak WSS values occurred in the marginal region as a result of rapid changes in arterial caliber and curvature, whereas the distal region exhibited relatively small WSS variations in response to large, relatively stable arterial curvatures. Both regions exhibited ΔWSS equivalent to or larger than those found in the proximal region with the inner- and outer-wall WSS values being higher.

No indications of steady flow separation or recirculation were seen in the model. As shown in Fig. 8, reasonable agreement was also found between the calculated WSS patterns (parabolic inlet profile) and those obtained experimentally for the same RCA geometry in Kirpalani *et al.*[17] with some localized differences in the portion of the marginal region where the marginal branch was removed. Both the experimental and numerical WSS distributions illustrate a large ΔWSS at locations greater than 0.2L from the cast origin.

Unsteady Flow: Variation in Inlet Velocity Conditions

Unsteady simulations produced axial and secondary velocity fields consistent with those found for steady flow. Specifically, varying the inlet velocity profile did not produce substantial changes in either the average WSS or ΔWSS, as illustrated in Fig. 9 for the WSS distributions from the fully developed (Womersley) and blunt inlet velocity profile simulations with the physiological waveform. As expected, the blunt inlet profile produced higher average WSS values on both the inner and outer RCA walls than found for the fully developed (Womersley) profile within the inlet region. However, these average distributions became indistinguishable distal to 0.2L. Consequently, the time-average WSS patterns closely resemble the steady WSS patterns illustrated in Fig. 7.

Unsteady Flow: Variation in Flow Waveform

Overall, the unsteady velocity fields differed only in response to each waveform's peak Reynolds number and negative flow interval, with qualitatively similar velocity distributions during intervals of equal flow. Variations in calculated WSS along inner RCA walls, plotted against normalized time, are shown in Fig. 10 for both the sinusoidal and physiological waveform (fully developed inlet profile). The outer-wall WSS distributions (not shown)

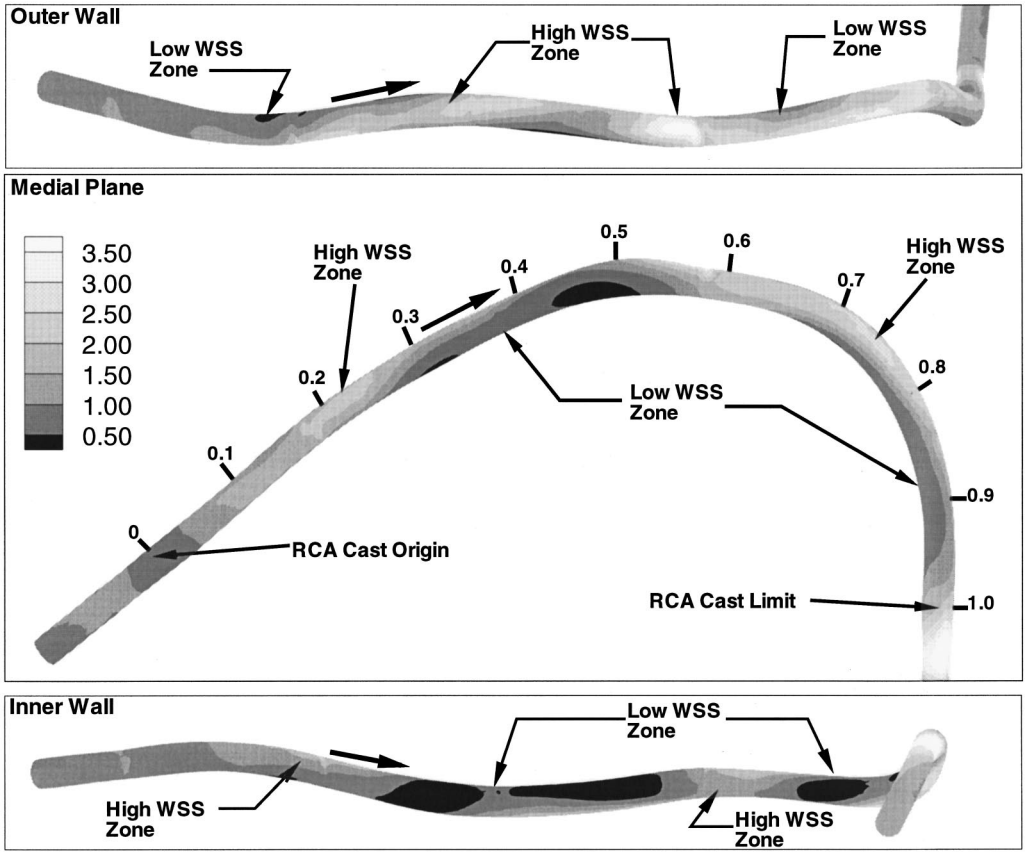

FIGURE 6. Contour plot of normalized WSS magnitude in the RCA model for steady flow with a Poiseuille inlet velocity profile. Note the alternating regions of high and low WSS on the model walls. WSS values are normalized by the inlet Poiseuille value.

were very similar for the peak flow periods of each waveform and did not show any flow separation. As expected, inner WSS values were lower than on the outer wall and also exhibited similar peak flow distributions. During deceleration in the sinusoidal waveform, localized regions of low (near-zero) WSS occurred along the inner wall of the proximal (0.26L), marginal (0.5L), and distal (0.72L, 0.96L) regions. Analogous features arose during each of the physiological waveform's deceleration phases. Each of these locations corresponds to a region with mainly medial plane curvature and an increasing arterial cross-sectional area, features that act to lower the local inner WSS by directing lower momentum fluid toward the inner wall.[15]

Although the lower momentum flow near the inner wall showed some sensitivity to adverse pressure gradients during flow deceleration, conditions were insufficient to cause local separation. For both flow waveforms, the calculated OSI never exceeded 0.05, with the primary contribution to OSI arising from the brief negative flow interval in the sinusoidal waveform. An OSI value this low is not considered physiologically significant.

The time-average WSS distributions between the sinusoidal and physiological waveform simulations, using the fully developed (Womersley) inlet velocity profile, were remarkably similar, differing primarily in magnitude and not in the prevailing pattern (Fig. 11). In general, the sinusoidal waveform exhibited higher average WSS values and inner/outer WSS differences ($\Delta WSS_{MAX} = 1.54$, $\Delta WSS_{AVG} = 0.423$) than did the physiological waveform ($\Delta WSS_{MAX} = 1.15$, $\Delta WSS_{AVG} = 0.312$). This similarity in the average WSS patterns is indicative of the significant role of the local arterial geometry, with the difference in magnitude attributed to the more pronounced positive flow interval of the sinusoidal waveform.

DISCUSSION AND CONCLUSION

This study was undertaken to characterize RCA hemodynamics and to examine if changes in the inlet velocity profile or flow waveform significantly influence important hemodynamic features (WSS, ΔWSS, and oscillatory WSS) in a physiologically faithful human RCA model. As discussed in more detail by Moore *et al.*,[26]

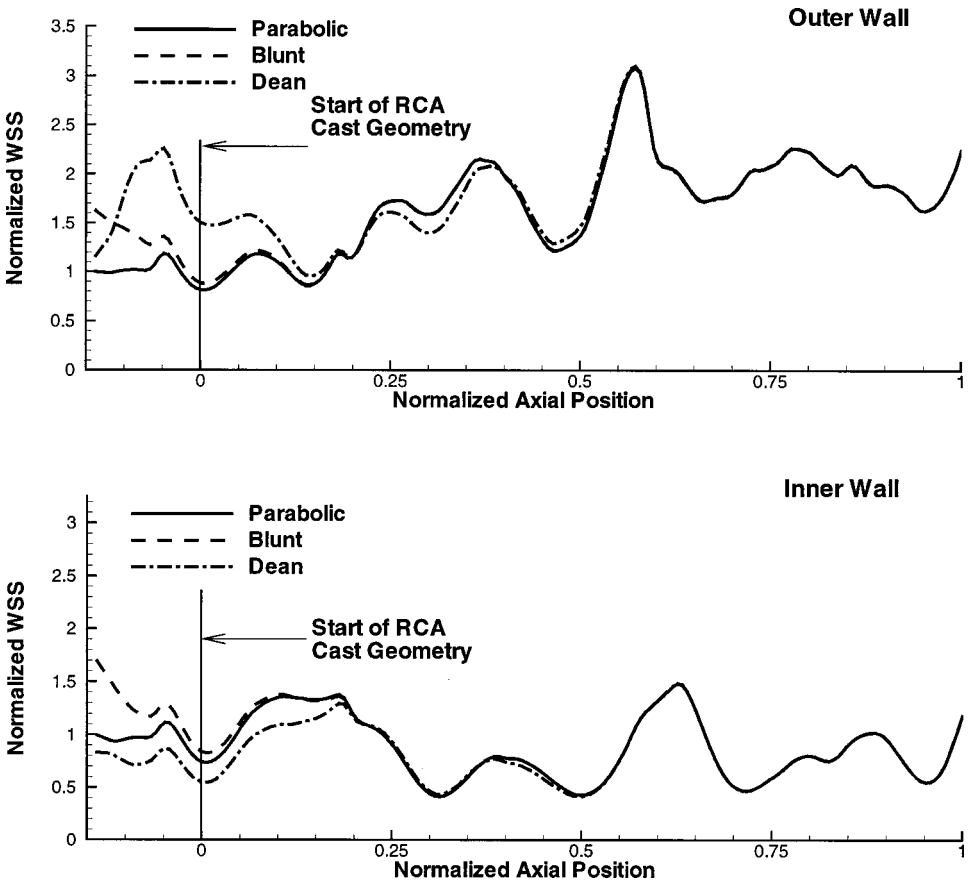

FIGURE 7. Effect of inlet profile on wall shear stress. WSS is normalized by the inlet Poiseuille value and plotted vs normalized arterial length along the outer (upper panel) and inner (lower panel) RCA wall.

WSS variations are considered significant only if they would lead to different conclusions regarding the link(s) between hemodynamics and coronary artery disease. Recent histological studies show that eccentric intimal thickening occurs predominantly along the inner wall of the RCA proximal region[29] and may be attributable to a combination of low WSS and large ΔWSS.[17] Conversely, the marginal and distal regions, which exhibit higher curvatures and more moderate WSS features, correlate to regions of uniform intimal thickening.[29] Therefore, our focus is on the inlet and proximal regions of the RCA.

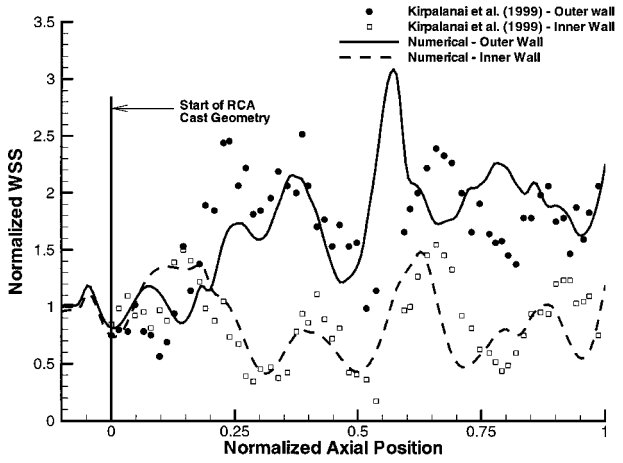

FIGURE 8. Comparison of calculated and experimental (Ref. 17) WSS distributions along the RCA inner and outer walls. A parabolic inlet velocity profile with $Re_D=500$ was used in both cases.

Our results show that the arterial geometry of the RCA was the dominant factor, dictating local velocity and WSS patterns for both steady and unsteady flow conditions. A particularly interesting hemodynamic effect was the ''rotation'' of the Dean-like secondary flow profiles due to out-of-plane curvature of the RCA model. Such Dean cell rotation due to compound curvature has been previously reported by Caro *et al.*[3] This produced alternating regions of high and low WSS on the sidewalls of the RCA model, which could be important in the localization of atherogenesis. These results show that there is a complex interaction between primary and secondary curvature in this RCA model, and that RCA hemodynamics are sensitive to local 3-D curvature effects.

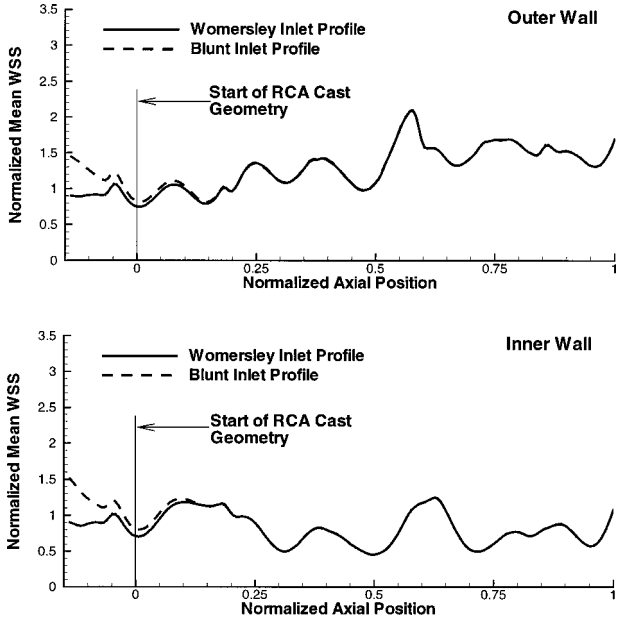

FIGURE 9. Comparison of normalized time-averaged WSS along the inner and outer walls of the RCA geometry, for different inlet velocity conditions (unsteady flow, physiologic waveform). Upper panel represents the RCA outer wall and the lower panel the inner wall. Solid line represents the Womersley inlet velocity profile, and dashed lines represent a flat inlet velocity profile.

In a previous study[26] in an end-to-side anastomosis geometry, it was observed that out-of-plane (secondary) curvature effects had a relatively minor effect on overall wall shear stress patters. At first sight this conclusion appears to be at variance with the results of the present study, but can be understood as follows. Most of the out-of-plane curvature seen in the end-to-side model was observed in the graft, in which there is relatively little primary curvature and a significant caliber enlargement due to the presence of a hood. As was noted in our earlier study,[26] removal of secondary curvature did produce some changes in the hood flow patterns, but these were largely overshadowed by effects due to the area expansion as the graft approaches the host artery. Distal to the graft–host mouth, the hemodynamics were almost completely dominated by the very drastic primary curvature associated with blood entry into the host, as well as the area changes in the host. Relative to these large effects, secondary curvature was negligible. Thus, it is clear that the importance of secondary curvature is model specific.[26]

In contrast to geometric effects, the inlet velocity profile did not substantially influence WSS beyond 9D from the cast origin, which is in agreement with the length scale required to achieve fully developed flow in planar-curved pipes, $[O(\sqrt{aR}) \sim 10\mathrm{D}]$.[31] The limited impact of the inlet velocity profile was primarily due to the low to

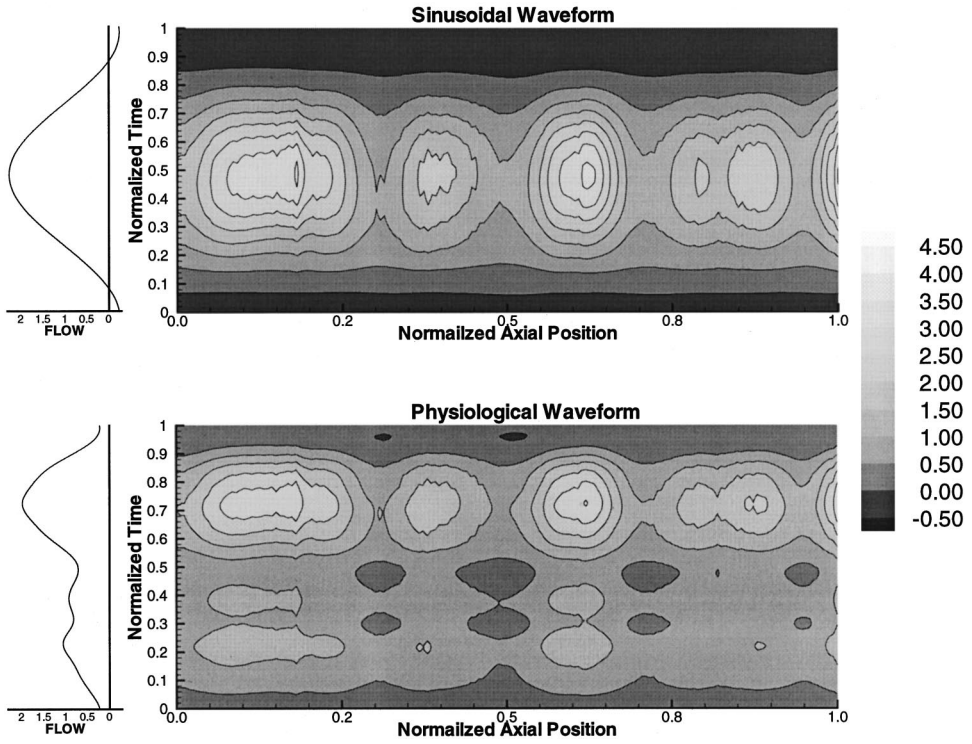

FIGURE 10. Normalized WSS distributions along the inner wall of the RCA throughout the sinusoidal (upper panel) and physiological (lower panel) waveform cycles. Note the WSS has been normalized using the inlet Poiseuille WSS value calculated at the mean-flow condition and the normalized axial position is relative to the artery's centroidal path.

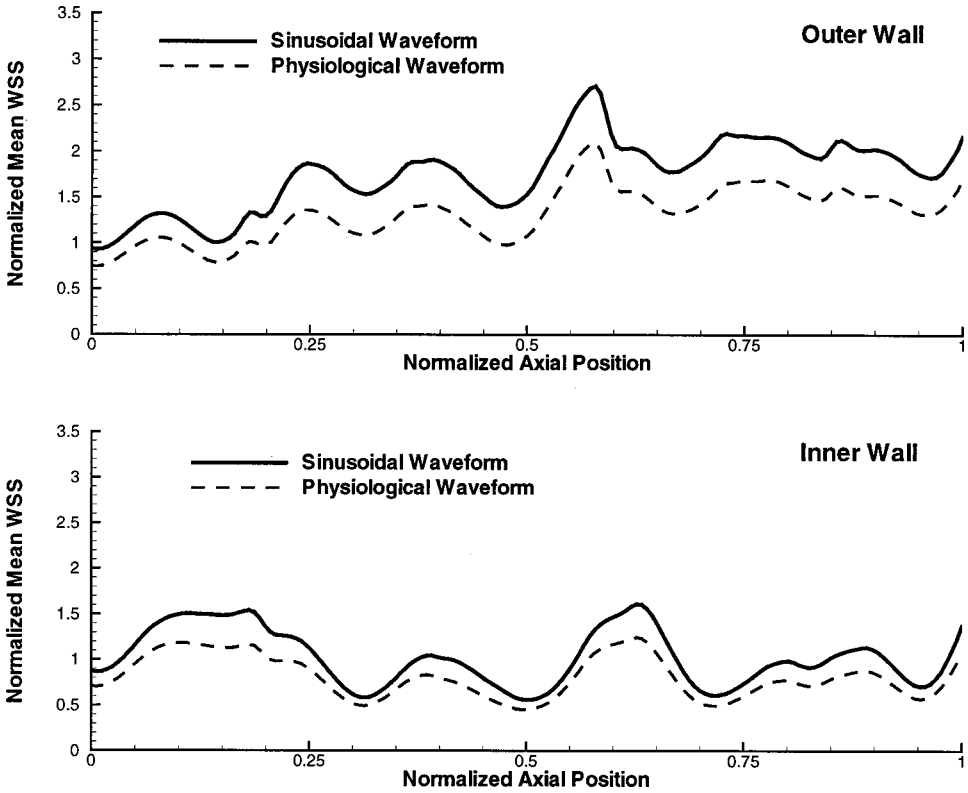

FIGURE 11. Comparison of mean normalized WSS values plotted vs normalized arterial length along the inner and outer walls of the RCA geometry from simulations using the Womersley (full-developed) inlet velocity profile. The top panel exhibits the WSS distributions for the RCA outer wall and the bottom panel exhibits the inner-wall WSS distributions. Solid lines represent the sinusoidal waveform and dashed lines represent the physiological waveform data. The similarity seen in both inner- and outer-wall cases is an indication of WSS dependence on the local RCA geometry.

moderately curved inlet and proximal regions of the RCA geometry inducing consistent cross-stream pressure gradients on the developing flow. Our inability to model the ostium and initial sections of the RCA did not substantially affect these observations. At the RCA model's inlet (2D from the ostium), blood flow will still be developing, exhibiting some secondary features,[2] and therefore the inlet profiles chosen for this study provide an overestimation of these effects.

For steady flow simulations, the Dean-type inlet profile induced flow features that were significantly different from those seen with the other inlet conditions. These significant differences were the result of the initial skewing of the velocity profile toward the outer wall, which increased the local outer-wall WSS and reduced the local inner-wall WSS. As the flow developed and responded to the changing arterial geometry, this effect became less significant with the weakened secondary flow resulting in minor differences (i.e., slightly lower WSS) along the outer wall for up to 50% of the artery length. Thus, overall, the significant effects of inlet (ostium) velocity profile were limited to the inlet region of the artery.

The effects of RCA geometry also dominated the WSS development for unsteady flows, limiting the propagation of significant inlet velocity profile effects. As a result, time-averaged WSS distributions were analogous to their steady flow counterparts, exhibiting similar overall trends and with significant inlet effects extending only into the RCA inlet region (0.2L). Therefore, unsteady flow simulations with the Dean-type inlet profile were deemed unnecessary, as we are reasonably confident that significant time-averaged WSS features are a function of the RCA geometry and can be extrapolated from analogous steady flow results.

Due to the geometric dependence of the flow field, time-averaged WSS distributions from each flow waveform exhibited remarkably similar patterns. Geometry dependence also limited the oscillatory features to those induced by reverse flow in each waveform. Although waveform dependence has been cited for flow in the aortic arch[5] and in an end-to-side anastomosis,[9] the results of this study imply that waveform shape is *not* a significant factor in the RCA time-averaged WSS features. As a consequence, idealized waveforms with peak, mean, and reverse-flow intervals similar to those of a physiologic waveform can provide physiologically relevant results.

A physiologically accurate geometry was utilized in this study, but the effects of branching and arterial movement, which can influence local flow separation and WSS patterns, were not considered.[17,35,37] The question of branch flows is particularly interesting, especially in light of the known variability of RCA anatomy and flow distribution. There is variability in the coronary circulation at a number of levels. Between individuals, it is well known that there is significant variability in which regions of the myocardium are served by the RCA (see, e.g., Fig. 5 of Zamir[41]). Zhou *et al.*[43] have argued that the coronary circulation follows a design constraint in which the caliber of a given arterial segment is determined by the length of the subtree supplied by that segment. This suggests that interindividual variations in branch caliber (and presumably flow rate) will directly follow variations in myocardial perfusion patterns. Between different regions within the same individual, there are also important differences. For example, King *et al.*[16] showed that the coefficient of variation for the flow distribution in the right ventricle was 32% in baboons. Some of this variation must be reflected in the caliber and flows within the branches that supply these different regions in the right ventricle, most of which will arise from the RCA. Taken together, this paints a picture of substantial patient-to-patient differences in branch caliber and flow, driven primarily by the anatomy of the arterial subtree supplied by each branch.

Given this variability, it is important to ask: how representative are our results? Ultimately, this depends on the importance of branch flows. In a separate publication[27] we show that branch flows are (somewhat surprisingly) not very important in determining wall shear stress patterns in the main trunk of the RCA. Taken together with the results of this paper, this implies that geometry is the major influence on RCA hemodynamics, and that accurate arterial geometries are an essential aspect of future RCA flow modeling studies.

ACKNOWLEDGMENTS

This work was supported by a NSERC Steacie Fellowship (C.R.E.), the R. Frasier Elliot Chair in Vascular Surgery (K.W.J.), and the Heart and Stroke Foundation of Ontario (M.O.).

REFERENCES

[1] Asakura, T., and T. Karino. Flow patterns and spatial distribution of atherosclerotic lesions in human coronary arteries. *Circ. Res.* 66:1045–1066, 1990.

[2] Berger, S. A., L. Talbot, and L. S. Yao. Flow in curved pipes. *Annu. Rev. Fluid Mech.* 15:461–512, 1983.

[3] Caro, C. G., D. J. Doorly, M. Tarnawaski, K. T. Scott, Q. Long, and C. L. Dumoulin. Nonplanar curvature and branching of arteries and non-planar-type flow. *Proc. R. Soc. London, Ser. A* 452:185–197, 1996.

[4] Caro, C. G., J. M. Fitz-Gerald, and R. C. Schroter. Atheroma and arterial wall shear. Observation, correlation and proposal of a shear-dependent mass transfer mechanism for atherogenesis. *Proc. R. Soc. London* 177:109–159, 1971.

[5] Chang, L., and J. M. Tarbell. Numerical simulation of fully developed sinusoidal and pulsatile (physiological) flow in curved tubes. *J. Fluid Mech.* 161:175–198, 1985.

[6] Davis, P. F. Flow-mediated endothelial mechanotransduction. *Physiol. Rev.* 75:519–560, 1995.

[7] Ding, Z., T. Biggs, W. A. Seed, and M. H. Friedman. Influence of the geometry of the left main coronary artery bifurcation on the distribution of sudanophilia in the daughter vessels. *Arterioscler., Thromb., Vasc. Biol.* 17:1356–1360, 1997.

[8] Ethier, C. R., D. A. Steinman, and M. Ojha. Comparison between computational haemodynamics, photochromic dye flow visualization and magnetic resonance velocimetry. In: Haemodynamics of Arterial Organs: Comparison of Computational Predictions with *In Vitro* and *In Vivo* Data, edited by X. Y. Xu and M. W. Collins. Southampton, UK: WIT, 1999, pp. 131–184.

[9] Ethier, C. R., D. A. Steinman, X. D. Zhang, S. R. Karpik, and M. Ojha. Flow waveform effects on end-to-side anastomotic flow patterns. *J. Biomech.* 31:609–617, 1998.

[10] Friedman, M. H., P. B. Baker, Z. Ding, and B. D. Kuban. Relationship between the geometry and quantitative morphology of the left anterior descending coronary artery. *Athero.* 125:183–192, 1996.

[11] Friedman, M. H., C. B. Bargeron, O. J. Deters, G. M. Hutchins, and F. F. Mark. Correlation between wall shear and intimal thickness at a coronary artery branch. *Athero.* 68:27–33, 1987.

[12] Friedman, M. H., O. J. Deters, F. F. Mark, C. B. Bargeron, and G. M. Hutchins. Arterial geometry affects hemodynamics. A potential risk factor for atherosclerosis. *Athero.* 46:225–231, 1983.

[13] He, X., and D. N. Ku. Pulsatile flow in the human left coronary artery bifurcation: Average conditions. *ASME J. Biomech. Eng.* 118:74–82, 1996.

[14] Holdsworth, D. W., M. Drangova, and A. Fenster. A high-resolution XRII-based quantitative volume CT scanner. *Med. Phys.* 20:449–462, 1993.

[15] Kaazempur-Mofrad, M. R., and C. R. Ethier. Mass transport in an anatomically realistic human right coronary artery. *Ann. Biomed. Eng.* 29:121–127, 2001.

[16] King, R. B., J. B. Bassingthwaighte, J. R. Hales, and L. B. Rowell. Stability of heterogeneity of myocardial blood flow in normal awake baboons. *Circ. Res.* 57:285–295, 1985.

[17] Kirpalani, A., H. Park, J. Butany, K. W. Johnston, and M. Ojha. Velocity and wall shear stress patterns in the human right coronary artery. *J. Biomech.* 121:1–6, 1999.

[18] Ku, D. N., D. P. Giddens, C. K. Zarins, and S. Glagov. Pulsatile flow and atherosclerosis in human carotid bifurcation: Positive correlation between plaque location and low and oscillating shear stress. *Arteriosclerosis* 5:293–302, 1985.

[19] Lee, B. K., H. M. Kwon, D. Kim, Y. W. Yoon, J. K. Seo, I. J. Kim, H. W. Roh, S. H. Suh, S. S. Yoo, and H. S. Kim. Computed numerical analysis of the biomechanical effects on coronary atherogenesis using human hemodynamics and dimensional variables. *Yonsei Med. J.* 39:166–174, 1998.

[20] Lynch, D. G., S. L. Waters, and T. J. Pedley. Flow in a tube with nonuniform, time-dependent curvature: Governing equa-

tions and simple examples. *J. Fluid Mech.* 323:237–265, 1996.
[21] Mark, F. F., C. B. Bargeron, O. J. Deters, and M. H. Friedman. Non-quasi-steady character of pulsatile flow in human coronary arteries. *J. Biomech. Eng.* 107:24–28, 1985.
[22] Matsuo, S., M. Tsuruta, M. Hayano, Y. Imamura, Y. Eguchi, T. Tokushima, and S. Tsuji. Phasic coronary artery flow velocity determined by Doppler flowmeter catheter in aortic stenosis and aortic regurgitation. *Am. J. Cardiol.* 62:917–922, 1988.
[23] Minev, P. D., and C. R. Ethier. A characteristic/finite-element algorithm for the Navier–Stokes equations using unstructured grids. *Comput. Methods Appl. Mech. Eng.* 178:39–50, 1999.
[24] Moore, J. A., D. A. Steinman, and C. R. Ethier. Computational blood flow modeling: Errors associated with reconstructing finite element models from magnetic resonance imaging. *J. Biomech.* 31:179–184, 1999.
[25] Moore, J. A., D. A. Steinman, D. W. Holdsworth, and C. R. Ethier. Accuracy of computational hemodynamics in complex arterial geometries reconstructed from magnetic resonance imaging. *Ann. Biomed. Eng.* 27:32–41, 1999.
[26] Moore, J. A., D. A. Steinman, S. Prakash, K. W. Johnston, and C. R. Ethier. A numerical study of blood flow patterns in anatomically realistic and simplified end-to-side anastomoses. *J. Biomech. Eng.* 121:265–272, 1999.
[27] Myers, J. G., M. Ojha, K. W. Johnston, and C. R. Ethier. Influence of branches, curvature, and caliber on blood flow patterns in the human right coronary artery. *Med. Biol. Eng. Comput.* (submitted).
[28] Nerem, R. M. Vascular fluid mechanics, the arterial wall, and atherosclerosis. *J. Biomech. Eng.* 114:274–282, 1992.
[29] Ojha M., R. L. Leask, J. Butany, and K. W. Johnston. Distribution of intimal and medial thickening in the human right coronary artery: A study of 17 RCA's. *Atherosclerosis* (in press).
[30] Pao, Y. C., J. T. Lu, and E. L. Ritman. Bending and twisting of an *in vivo* coronary artery at a bifurcation. *J. Biomech.* 25:287–295, 1992.
[31] Pedley, T. J. The Fluid Mechanics of Large Blood Vessels. Cambridge: Cambridge University Press, 1980.
[32] Perktold, K., M. Hofer, G. Rappitsch, M. Loew, B. D. Kuban, and M. H. Friedman. Validated computation of physiologic flow in a realistic coronary artery branch. *J. Biomech.* 31:217–228, 1998.
[33] Perktold, K., R. M. Nerem, and R. O. Peter. A numerical calculation of flow in a curved tube model of the left main coronary artery. *J. Biomech.* 24:175–189, 1991.
[34] Prakash, S., and C. R. Ethier. Requirements for mesh resolution in 3-D computational hemodynamics. *ASME J. Biomech. Eng.* (in press).
[35] Qiu, Y., and J. M. Tarbell. Numerical simulation of pulsatile flow in a compliant curved tube model of a coronary artery. *J. Biomech. Eng.* 122:77–85, 2000.
[36] Sabbah, H. N., F. Khaja, J. F. Brymer, E. T. Hawkins, and P. D. Stein. Blood velocity in the right coronary artery: Relation to the distribution of atherosclerotic lesions. *Am. J. Cardiol.* 53:1008–1012, 1984.
[37] Santamarina, A., E. Weydahl, J. M. Siegel, and J. E. Moore. Computational analysis of flow in a curved tube model of the coronary arteries: Effects of time-varying curvature. *Ann. Biomed. Eng.* 26:944–954, 1998.
[38] Schilt, S., J. E. Moore, A. Delfino, and J. J. Meister. The effects of time-varying curvature on velocity profiles in a model of the coronary arteries. *J. Biomech.* 29:469–474, 1996.
[39] Singh, M. P. Entry flow in a curved pipe. *J. Fluid Mech.* 65:517–539, 1974.
[40] Yutani, C., M. Imakitaa, Ishibashi-Ueda, A. Yamamoto, and S. Takaichi. Localization of lipids and cell population in atheromatous lesions in aorta its main arterial branches in patients with hypercholesterolemia. In: Role of Blood Flow in Atherogenesis, edited by Yoshida *et al.* Tokyo: Springer, 1988.
[41] Zamir, M. Flow strategy and functional design of the coronary network. In: Coronation Circulation: Basic Mechanism and Clinical Relevance, edited by F. Kajiya, G. A. Klassen, J. A. E. Spaan, and J. J. E. Hoffman. Tokyo: Springer, 1990, pp. 15–40.
[42] Zarins, C. K., M. A. Zatina, D. P. Giddens, D. N. Ku, and S. Glagov. Shear stress regulation of artery lumen diameter in experimental atherogenesis. *J. Vasc. Surg.* 5:413–420, 1987.
[43] Zhou, Y., G. S. Kassab, and S. Molloi. On the design of the coronary arterial tree: A generalization of Murray's law. *Phys. Med. Biol.* 44:2929–2945, 1999.